Enhancing Hybrid Exoskeleton Performance with Spatially Distributed Asynchronous Stimulation and Ultrasound Imaging-based Fatigue Measurements

Ashwin Iyer, Vidisha Ganesh, Mayank Singh, William Filer, Christine Cleveland, Nitin Sharma

***Abstract*—This paper introduces an innovative approach, Spatially distributed asynchronous stimulation (SDAS), designed to enhance the fatigue resistance of electrically stimulated muscles for mobility assistance in individuals with spinal cord injury (SCI), stroke, and multiple sclerosis. The study focuses on modulating stimulation intensity in multiple distributed electrodes through a phenomenological model of SDAS to increase muscle power output. A model predictive control (MPC) approach is used to design optimal SDAS intensity profiles for knee extension tracking. The study also establishes a strong correlation between Ultrasound (US)-derived strain measurements of the quadriceps muscle and the model's fatigue parameter. The model is extended to predict non-isometric knee extension and integrated with US-derived feedback from the quadriceps muscle to control stepping with the hybrid exoskeleton. The results demonstrate that the optimized SDAS inputs and US-derived fatigue measurements of spatially separated muscle regions during SDAS can effectively delay fatigue and increase muscle power output. This study underscores the importance of a model-based closed-loop SDAS approach and the integration of US-derived feedback in the design of a novel fatigue-resistant SDAS-based gait assistance technology.**

I. Introduction

Functional electrical stimulation (FES) is a therapeutic technology that enhances motor function in individuals with spinal cord injury (SCI), stroke, and multiple sclerosis [1], [2]. The technology delivers electrical impulses to the muscles through surface electrodes, which evoke muscle contractions, promote movement, and assist in daily activities such as walking [3]. FES can mitigate muscle atrophy and improve circulation, while some individuals may benefit from enhanced motor recovery and reduced spasticity. Despite its potential, FES faces a significant limitation due to the quick onset of FES-induced muscle fatigue, which limits the duration of FES use and its effectiveness at performing functional tasks.

Proposed solutions to delay the fatigue onset include designing optimal stimulation protocols [4], fine-tuning the electrode placement to influence the muscle power output [5]–[7], and modulating stimulation parameters, such as frequency, pulse width, and current amplitude [7]–[12]. In [7], reducing stimulation frequency resulted in better fatigue resistance (i.e., less sharp power decay) but significantly lower power output (peak power). Instead, asynchronous stimulation of spatially distributed electrodes (SDAS) can generate high power and reduce fatigue [13]–[15]. Unlike the traditional FES approach, which uses an electrode pair on the quadriceps, SDAS uses multiple electrodes to stimulate individual muscles of the quadriceps, mainly the *Vastus medialis (VM)* and *Vastus lateralis (VL)*. SDAS uses multiple smaller electrodes, instead of a single large electrode, grouped at a common location. This clustered multi-electrode approach activates partially distinct muscle sub-compartments, potentially recruiting separate motor unit population. Thus, compared to a single electrode use, SDAS ideally reduces discharge rates of each motor unit population and, consequently, muscle fatigue. The SDAS studies have shown increased fatigue resistance and power output in both isometric and non-isometric settings on participants with and without disability [16]–[20].

Recently, in addition to FES, hybrid exoskeletons that augment powered exoskeletons with electrical stimulation have been shown to provide lower limb mobility [21]–[23]. Various control methods ranging from proportional-integral-derivative combined with muscle torque estimation [24], event-based triggering [25] model predictive control (MPC) [26]–[28], and switching between motor and FES [29] have helped perform a variety of movements involving quadriceps muscles including continuous knee extension, sit-to-stand, and stepping.

However, augmenting a hybrid exoskeleton with SDAS in open-loop or closed-loop remains unexplored. Recent studies investigated open-loop SDAS during knee or an ankle dynamometery [15]–[18], [20], [30]. Non-isometric conditions with SDAS, such as rowing [19] and cycling [31], have also been studied to quantify force production improvements over traditional FES but remain in an open-loop setting. Closed-loop SDAS design was proposed by Downey et al. [32], who designed a switching control design that determines inputs to each electrode in an asynchronous stimulation configured to elicit seated continuous knee extension. Knee extension tracking on non-disabled participants showed that the asynchronous closed-loop control scheme delays the impact of fatigue. While this closed-loop approach is effective at tracking a desired knee joint trajectory, closed-loop SDAS designs that modulate the inputs based on a measured muscle fatigue state are lacking. Closed-loop SDAS with fatigue as feedback would be especially meaningful in a hybrid exoskeleton where the fatigue estimates are crucial to modulate exoskeleton assistance to compensate for the FES-induced fatigue .

Current sensing mechanisms to measure muscle fatigue include force measurements using a load cell or dynamometer [33] and surface electroymography (sEMG) [34]–[36]. However, using load a force measurement in real-time is challenging as it is difficult to estimate force in a dynamic setting. Most dynamometers and load cells are not portable

for real-time exoskeleton control and measure the cumulative output of a muscle group at a specific joint. Force measurements of sub-muscle groups within a larger muscle group such as the quadriceps is usually non-trivial to decompose [35]. Utilizing sEMG is also challenging as it is sensitive to electrode placement, and is susceptible to signal interference from FES and cross talk between neighboring muscles [37].

Alternatively, US imaging techniques have recently been proposed to study the muscle contraction behavior in neuromuscular systems [38]–[43]. US imaging can directly visualize desired muscles without interference from FES or neighboring muscle activity while providing a wide variety of signals such as muscle thickness, pennation angle, and fascicle length. These can then be used to analyze muscle contractility of sub muscle groups within a larger muscle group, predict human motion [44]–[46], and be incorporated into real-time control of an assistive device [47]. Additionally, we showed in our recent studies [48], [49] that the axial strain derived from US images is a promising indicator of contractility change in the human quadriceps muscles due to FES-induced fatigue. US images were captured during isometric muscle contractions generated by FES, and a strain tensor was computed based on estimates of tissue motion in the captured images. Specifically, we showed the correlation between force output of the quadriceps with strain changes in the *VI* during the traditional stimulation approach. This measurement scheme has also been integrated into a closed-loop control of a hybrid exoskeleton [50], [51].

This paper aims to develop and integrate an SDAS model into a hybrid exoskeleton using an MPC scheme with real-time US-derived fatigue state measurements. The integration of real-time US imaging into a hybrid exoskeleton with SDAS is achieved through the following contributions:

- We propose a modified Hill-Huxley model that accounts for stimulation intensity during SDAS to predict the forces generated by both the *VL* and *VM* in an isometric setting
- We investigate the use of US imaging in the proposed model by investigating the relationship between the fatigue properties of each muscle from the model and those measured from US images.
- We develop an MPC approach that determines the optimal stimulation current intensity required to generate a desired force and verify the results experimentally on participants with SCI and without disability
- We extend the proposed isometric model to a dynamic walking task of the swing phase and show, for the first time, real-time US imaging during SDAS in conjunction with a powered exoskeleton on two participants with SCI and one participant with no disability.

The rest of this article is organized as follows: Section II presents the modified Hill-Huuxley model during SDAS in both isometric and dynamic settings. Section III presents the experimental validation of the proposed model. Section IV shows the integration of US imaging into the proposed models, and Section IV shows SDAS walking in a hybrid exoskeleton. Section V presents the discussion. Finally, Section VI concludes this article.

II. Modified Hill-Huxley Model for SDAS

To develop closed-loop control methods that modulates stimulation intensity, we modify an isometric force generation model, first proposed in [52]. The modified model predicts the isometric force exerted, $F_{pj} \in \mathbb{R}$, by each electrode $j \in \mathbb{Z}^+$ at muscle $p \in [VM, VL]$ in a SDAS setup as

$$\frac{dF_{pj}}{dt} = A_p \frac{\bar{C}_{N_{pj}}}{K_{mp} + \bar{C}_{N_{pj}}} - \frac{F_{pj}}{\tau_{1p} + \tau_{2p} \frac{\bar{C}_{N_{pj}}}{K_{mp} + \bar{C}_{N_{pj}}}}, \quad (1)$$

where $A_p \in \mathbb{R}$ is a scaling factor of the stimulated muscle driven by the following dynamics

$$\frac{dA_p}{dt} = -\frac{A_p - A_{p0}}{\tau_{fp}} + \alpha_p F_{pj}, \quad (2)$$

where $\alpha_p \in \mathbb{R}$ and $\tau_{fp} \in \mathbb{R}$ are fatigue and recovery time constants and $A_{p0} \in \mathbb{R}$ is an initial condition for A_p during an isometric contraction when the leg is held at 0 degrees from the vertical. $\tau_{1p} \in \mathbb{R}$ and $\tau_{2p} \in \mathbb{R}$ in (1) are muscle-specific time constants, $K_{mp} \in \mathbb{R}$ represents the sensitivity of force generation calcium dynamics. $\bar{C}_{Npj} \in \mathbb{R}$ is defined as

$$\bar{C}_{N_{pj}} = u_j C_{N_{pj}} \quad (3)$$

to account for stimulation intensity, where $u_j \in \mathbb{R}$ is a stimulation intensity (current or pulse width) normalized between user-specific threshold and saturation and $C_{Npj} \in \mathbb{R}$ represents the calcium dynamics of the muscle due to contributions from electrode j defined as

$$\begin{gathered} \frac{dC_{N_{pj}}}{dt} = \frac{1}{\tau_c} \sum_{i=1}^{n} R_i e^{(-\frac{t-t_i}{\tau_c})} - \frac{C_{N_{pj}}}{\tau_c} \\ R_i = 1 + (R_{0p} - 1) e^{(\frac{t-t_i}{\tau_c})} \end{gathered} \quad (4)$$

where $t_i \in \mathbb{R}^+$ is the time of i^{th} stimulation pulse, $n \in \mathbb{Z}^+$ is the number of stimuli in the pulse train before time instant t, $R_{0p} \in \mathbb{R}$ is a constant that determines the magnitude of activation based on successive stimulation pulses, and $\tau_c \in \mathbb{R}$ is a calcium dynamics time constant. The modified model in (1) can be scaled in dimension to match the number of electrodes targeting each muscle and the total force, $F \in \mathbb{R}$, generated is a sum of the individual forces of each muscle computed as

$$F = \sum_{j=1}^{N_{vl}} F_{jvl} + \sum_{j=1}^{N_{vm}} F_{jvm}, \quad (5)$$

where $N_{vm} \in \mathbb{Z}^+$ and $N_{vl} \in \mathbb{Z}^+$ are the number of electrodes targeting the *VL* and *VM* respectively.

To account for a non-isometric motion, we adapt the model in [53] and define the total force of the quadriceps in an SDAS as

$$\frac{dF_{pj}}{dt} = [\vartheta(\theta)\dot{\theta} + \lambda(\theta)][A_p \frac{\bar{C}_{N_{pj}}}{K_{mp} + \bar{C}_{N_{pj}}} - \frac{F_{pj}}{\tau_{1p} + \tau_{2p} \frac{\bar{C}_{N_{pj}}}{K_{mp} + \bar{C}_{N_{pj}}}}], \quad (6)$$

where $\lambda(\theta) \in \mathbb{R}$ and $\vartheta(\theta)\dot{\theta} \in \mathbb{R}$ represent force length and force velocity terms, respectively. $\lambda(\theta)$ is defined as

$$\lambda(\theta) = \lambda_1 (40 - \theta)^2 + \lambda_2 (40 - \theta) + A_{p40} \quad (7)$$

Table I: Participant Demographics

Participant	Age	Gender	Injury Level
B1	20	F	N/A
B2	26	F	N/A
S1	52	M	T10, incomplete
S2	60	M	T7, complete

where A_{p40} is the value for A_p in (2) when the knee was held at 40 degrees and all other parameters were held constant and λ_1 and λ_2 are model parameters to be identified. Further, $\vartheta(\theta)$ is defined as

$$\vartheta(\theta) = \bar{\vartheta} e^{([\frac{3.0523}{\tau_2} - .0574]\theta)}, \tag{8}$$

where $\bar{\vartheta} \in \mathbb{R}$ is a person specific model parameter. It is noted that when the knee is suspended vertically at zero degrees from the vertical and $\dot{\theta} = 0$, (6) is same as the general isometric model in (1). Further, for nonisometric motion, the knee extension dynamics during SDAS can written as

$$J\ddot{\theta} + T_p(\theta, \dot{\theta}) + G(\theta) = T_{stim}, \tag{9}$$

where $\theta, \dot{\theta}, \ddot{\theta} \in \mathbb{R}$ represent the angular position, velocity, and acceleration of the knee joint, $J \in \mathbb{R}^+$ is the moment of inertia of the leg, and $G(\theta) = mglsin(\theta + \theta_{eq})$ is a term that represents the torque due to gravity where $m \in \mathbb{R}^+$ is the mass of the lower leg, g is the gravitational acceleration constant, l is defined as half the length of the users shank, and $\theta_{eq} \in \mathbb{R}^+$ is the equilibrium position of the lower leg with respect to the vertical. T_p is the passive torque of the knee joint and is modeled as $T_p(\theta, \dot{\theta}) = d_1(\phi - \phi_0) + d_2\dot{\phi} + d_3 e^{d_4\phi} - d_5 e^{d_6\phi}$, where $\phi, \dot{\phi}$ are the anatomical knee joint angle and angular velocity defined as $\phi = \frac{\pi}{2} - \theta - \theta_{eq}, \dot{\phi} = -\dot{\theta}$, and $d_i (i = 1, 2, ...6) \in \mathbb{R}$ are person specific parameters and $T_{stim} = Fl$ where is the total force of the quadriceps defined in (5).

III. Model Validation

The experiments in this section aim at validating the model in (1). Four participants (2 SCI, 2 no disability) were recruited to participate in four experimental sessions in which they were seated in a dynamometer (Biodex) to measure isometric torque output. When seated, the lower leg was suspended and secured to the dynamometer at an approximately 90 degree angle using a knee attachment. To characterize force production of the quadriceps, the measured torque was converted to force based the length between the center of rotation of the knee and point at which the knee attachment was secured to the leg. All protocols were approved by the institutional review board (IRB) at North Carolina State University. Details on each participant is shown in Table I. All protocols were repeated on both legs of all participants for a total of 8 legs. Table II details all the experimental sessions.

A. Stimulation Procedures

At the beginning of the first session, saturation and threshold current amplitudes for each participant were determined by ramping current up in 2mA increments between 20mA and 70mA (or maximum current level at which participant is comfortable) and recording the force production of the quadriceps. The threshold was defined as the current amplitude at which a noticeable force was measured. The saturation was defined as the current at which the measured force no longer increased. For the rest of the study, all stimulation inputs were normalized between the saturation and threshold values. Both the traditional and SDAS protocols were administered at a current level that was 85% of the saturation along with a $300\mu S$ pulse width. Stimulation was achieved using a commercial stimulator (Rehastim 2, HASOMED GmbH, Germany) at a desired frequency, pulse width, and current. For the traditional FES approach, two large electrodes (PALS, 7.62 cm by 10.16 cm, Axelgaard Manufacturing Co., Ltd., USA) were placed on the quadriceps. During SDAS two smaller square electrodes (PALS, 5 cm by 5 cm, Axelgaard Manufacturing Co., Ltd., USA) were placed around both *VL* and *VM* with a two common large electrodes for the *VL* and *VM* respectively as seen in Fig. 1. The electrodes were stimulated at a frequency of 20 hz with a .025 second phase delay such that the corresponding frequency for each muscle was 40 hz. The fatiguing protocol for both approaches in this study consists of repeated 1.5 second pulse stimulation pulse trains with a rest of 0.5 seconds for a duration of 120 seconds. Fig. 2 highlights the fatiguing protocol used in both the traditional and SDAS approaches.

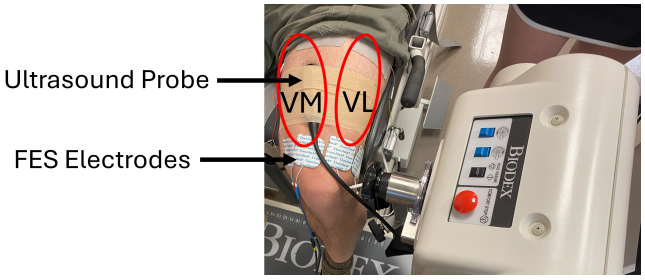

Figure 1: SDAS and US imaging setup to stimulate both the VL and VM. Participants were seated in the dynamometer with their leg suspended at a 90 degree angle and the force output during a stimulation protocol was recorded.

B. Isometric Parameter Identification

It is seen from (1) and (2) that for each muscle, there are seven unknown parameters in the isometric force model: $R_{0p}, \tau_{1p}, \tau_{2p}, K_{mp}, A_{p0}, \alpha_p, \tau_{fp}$. These parameters were identified by using the force measurements during which only one muscle was stimulated using the SDAS isometric fatiguing protocol collected in session 2. The parameters $R_{0p}, \tau_{1p}, \tau_{2p}, K_{mp}, A_{p0}$ were determined based on the measured force, F_m, from the first five stimulation cycles of the protocol to ensure the muscle had yet to fatigue. These parameters were estimated by solving the optimization problem

$$\min J = \frac{1}{n} \sum_{i=1}^{n} (F_p(i, u_j) - F_m)^2 \tag{10}$$

where $F_p(n, u_j)$ is the predicted force at sample point n from (5) during the first five stimulation cycles given a stimulation intensity for each pad u_j. $F_p(n, u_j)$ was determined by solving

Session	Description	Number of participants
1	Traditional electrode fatiguing protocol	4
2	SDAS isometric parameter identification	4
3	SDAS fatiguing protocol	4
4	SDAS model validation protocol	4
5	SDAS nonisometric parameter	3

Table II: IIDetails on experimental sessions

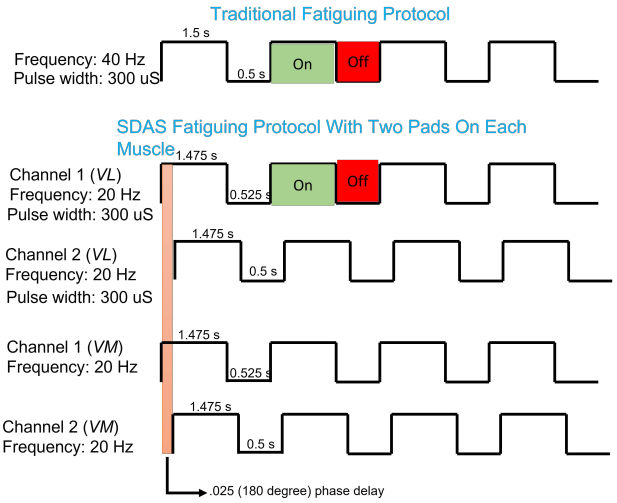

Figure 2: Fatiguing protocol for both the traditional setup and SDAS. The overall protocol consists of 60 1.5 second contractions with 0.5 seconds of rest in between. The SDAS protocol consists of two electrodes on the *VL* and *VM* and stimulated at a lower frequency with a phase delay such that the corresponding frequency to each muscle matches the total frequency.

(1) based on the the calcium dynamics of each electrode j replacing A_p with A_{p0} since only the first five cycles are considered.

Once the parameters $R_{0p}, \tau_{1p}, \tau_{2p}, K_{mp}, A_{p0}$ are determined, α_p and τ_{fp} are estimated by minimizing the cost function in (10) over the whole fatiguing protocol. All optimizations were performed using fmincon, a nonlinear optimization problem solver in MATLAB. Once the model parameters were identified, we performed an SDAS fatiguing protocol while stimulating both the *VL* and *VM* in session 3 and compared the predicted force output to the measured force during SDAS in which both the VL and VM are stimulated. For each contraction in the stimulation protocol, we computed the force-time-integral (FTI) for both the measured force response during SDAS and the predicted force response based on parameter identification for both the VL and VM. Fig. 3 shows the FTI for both legs of participant S2. The FTI for each leg of each participant is shown in Table III. The average R^2 value between FTI and measured force for both legs of all participants was $0.87 \pm .03$.

C. Offline MPC to Perform a Force Tracking Task

In this section, we propose and validate an MPC framework to track a desired isometric force profile during SDAS based on the model in (1) and ensure that each muscle contributes equally to the total force generated. In this case, we consider a two pad SDAS approach in which two electrodes are placed on both the *VL* and *VM*. Thus, the system state, $x \in \mathbb{R}^6$, and control input, $u \in \mathbb{R}^4$ are defined as $x = \begin{bmatrix} x_1 & x_2 & x_3 & x_4 & x_5 & x_6 \end{bmatrix} = \begin{bmatrix} F_{vm1} & F_{vm2} & A_{vm} & F_{vl1} & F_{vl2} & A_{vl} \end{bmatrix}^T$ and $u = \begin{bmatrix} u_1 & u_2 & u_3 & u_4 \end{bmatrix}^T$ where $u_1 \in \mathbb{R}$ and $u_2 \in \mathbb{R}$ contribute to the *VM* and $u_3 \in \mathbb{R}$ and $u_4 \in \mathbb{R}$ contribute to the *VL*.The MPC framework solves the following optimal control problem on prediction horizon T

$$\min_u \int_0^T l(x,u)d\tau \tag{11}$$

subject to :

$$\dot{x} = f(x,u)$$

$$0 \leq u_f \leq 1$$

where $\dot{x} = f(x,u)$ is the state space form of the dynamics defined in (1) and (2) and $l(x,u) \in \mathbb{R}$ is the cost defined as

$$l(x,u) = Q_1(F_{vmd} - (x_1 + x_2))^2 + Q_2(F_{vld} - (x_4 + x_5))^2 + R_1u_1^2 + R_2u_2^2 + R_3u_3^2 + R_4u_4^2$$

where $Q_1, Q_2, R_1..R_4 \in \mathbb{R}^+$ are positive weights, and $F_{vmd} \in \mathbb{R}$ and $F_{vld} \in \mathbb{R}$ are the desired forces of the VL and VM respectively.

We performed simulations to show the predicted force output when using the MPC framework to track a desired force, designed as sixty step functions with length of 1.5 seconds and 0.5 seconds rest. The optimal inputs on the prediction horizon T are solved using a fast gradient projection algorithm [54]. The desired force for each leg of each participant was determined by taking the average total force produced during the first 5 contractions when the SDAS fatiguing protocol was applied. Fig. 4 shows the peak force generated during each of the 60 contractions over the two minute duration for the right leg of each participant with SCI along with contributions of

Table III: R^2 value when comparing FTI of predicted force from the model versus measured force from the isometric SDAS stimulation protocol

Participant	Leg	R^2
B1	R	0.84
	L	0.86
B2	R	0.85
	L	0.9
S1	R	0.92
	L	0.89
S2	R	0.88
	L	0.86

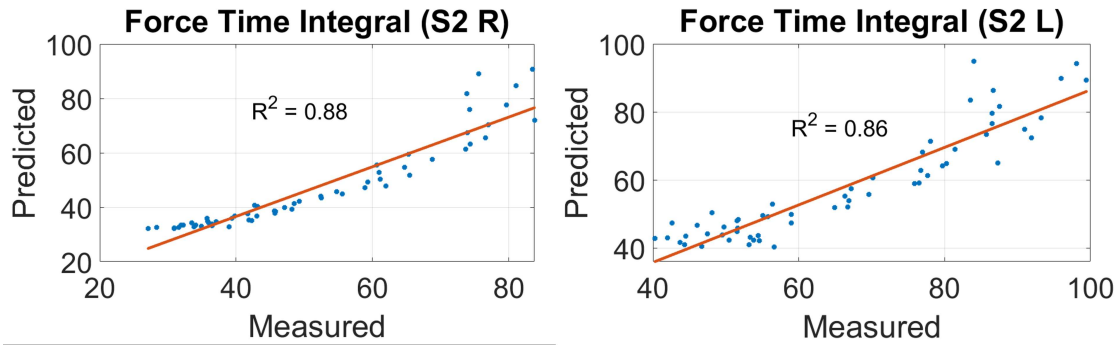

Figure 3: Predicted versus measured FTI for the right leg of participant S2 (SCI) along with their respective R^2 values

the *VL* and *VM* and the integrals of normalized FES inputs at each contraction for each electrode. It can be seen that the desired force was initially maintained before the both the *VL* and *VM* start to fatigue. Additionally, the inputs to each electrode show that as the *VL* and *VM* fatigued, the stimulation input increases and eventually saturates. An additional set of simulations were performed where the desired force for the two minute fatiguing protocol was set at a constant 30 N. Fig. 4 shows representative tracking and inputs and it is clear that when the desired force is lower, better force performance is achieved.

To validate the simulation results, in session 4, we applied the optimal stimulation intensities calculated by the MPC framework. The desired force was set to match the non-fatigue force generation of the SDAS protocol with constant current for each participant. For each stimulation protocol (traditional, SDAS with constant intensity, MPC) we computed two metrics: mean force output ($F_{mean} \in \mathbb{R}$) and force decay ($F_{decay} \in \mathbb{R}$). For each contraction in the fatiguing protocol, we determined the generated peak force. F_{mean} was then computed as the average peak force over the 60 contractions. To compute F_{decay}, we computed the max force, $F_{max} \in \mathbb{R}$, as the average force during the first five contractions and the fatigued force, $F_{fat} \in \mathbb{R}$, was defined as the average force during the final ten contractions. We then calculated the power decay as

$$F_{decay} = 100 - (F_{fat}/F_{max}) * 100.$$

F_{mean} for all participants is shown in Fig. 5. It is seen that the F_{mean} increases when using SDAS with constant current compared to the traditional approach and further increases with SDAS with MPC for all participants. Individual results for F_{mean} are shown in Table IV. On comparing the fatigue properties of the three approaches, the average F_{decay} among both the legs of all participants was 76.94 ± 9.43, 61.55 ± 8.63 and 49.58 ± 12.82 N for the traditional stimulation approach, SDAS with constant current, SDAS with MPC respectively. We performed an Analysis of Variance (ANOVA) that revealed a significant difference in F_{decay} among the three protocols ($F = 13.75, p < .001, \alpha = 0.95$). Values for F_{decay} Table IV for all participants.

We further compared the experimental force output to the force output from simulations under the same optimal inputs. The average root mean squared error (RMSE) for all participants between the simulation and experiment was 7.41 ± 1.86 N.

IV. Incorporation of US-image derived fatigue measures into proposed model

A. Ultrasound Imaging-Derived Fatigue Measurement

In [48], a speckle tracking algorithm was developed to measure tissue motion during FES-induced contractions of the quadriceps. It was observed that as the quadriceps fatigued, a decay in tissue motion captured by the algorithm is correlated with the decay in force output from the quadriceps measured by a load cell. The speckle tracking algorithm is based on a displacement matrix $d_{m,n}(x, y)$ between two images m and n in the axial(depth) and lateral(width) directions at each spatial position in a region of interest (ROI) of a specific muscle group. The ROI varies for each participant depending on the muscle architecture chosen based on the placement of the US probe on the body such that during a sequence of images captured during a isometric motion of the limb, a majority of the imaged muscle stays in the view of the probe and does not translate off the image. When imaging the quadriceps, the ROI is typically between 10mm to 45mm deep and spans 10 mm in the center of the image. The displacement matrix is calculated as

$$d_{m,n}(x, y) = arg\max_{u,v}(\gamma(u, v)),$$

where

$$\gamma(x, y) = \frac{\sum_{K_{x,y}}(f_m(a, b) - \bar{f}_m)(f_n(a + u, b + v) - \bar{f}_{n,u,v})}{\sqrt{\sum_{K_{x,y}}(f_m(a, b) - \bar{f}_m)^2(f_n(a + u, b + v) - \bar{f}_{n,u,v})^2}}$$

where a, b are all all the spatial locations in a kernel $K_{a,b}$centered at each point (x, y) in the ROI such that $(a, b) \in K_{a,b}$ and u, v are all the spatial locations in a search window $K_{u,v}$centered at each location (a, b) such that $(u, v) \in K_{u,v}$. Furthermore, f_m and f_n are the US image intensity of the reference and current image respectively and $\bar{f}_m$ and $\bar{f}_n$ are averaged values of $f_m(a, b)$ and $f_n(a + u, b + v)$. We spatially filter $d_{m,n}(x, y)$ to mitigate tracking noise between each pair of frames. A $M \times N$ pixel kernel was generated and centered around (x, y). The median value of $d_{m,n}(x, y)$ within the kernel was assigned to a filtered displacement map

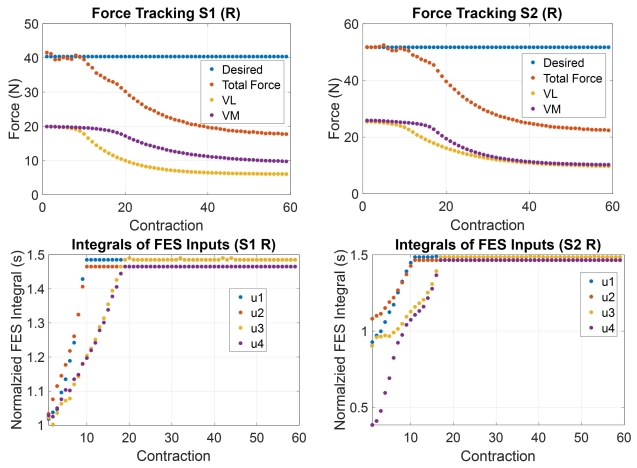

(a) The desired force determined by taking the average force of the first 5 contractions when the SDAS protocol was administered.

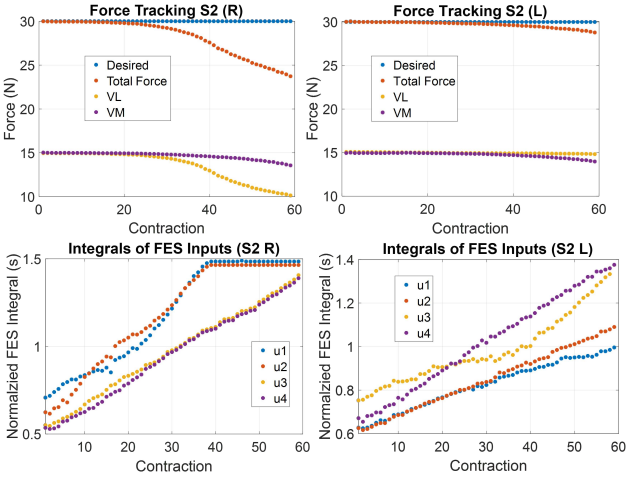

(b) The desired force set to 30 N

Figure 4: Force tracking results for the right leg of each participant with SCI under different desired force conditions highlighting the desired force and contributions of both VL and VM to the total force for each participant along the respective integrals of inputs at each contraction.

Table IV: Average force output and force decay under each stimulation condition

Participant	Leg	Traditional		SDAS (Constant)		SDAS (MPC)	
		Average Force Output (N)	F_{decay}	Average Force Output (N)	F_{decay}	Average Force Output (N)	F_{decay}
S1	L	11.90	90.80	18.89	65.85	26.37	66.67
	R	15.49	91.18	18.09	76.66	27.31	55.34
S2	L	21.2	75.50	43.27	52.29	45.19	47.07
	R	15.76	77.29	32.83	60.91	36.21	56.11
B1	L	18.36	67.11	38.48	61.86	43.43	56.14
	R	14.92	75.74	24.35	66.21	27.84	41.32
B2	L	23.87	68.76	41.11	59.68	51.91	50.23
	R	39.49	69.12	60.38	48.34	66.30	23.78

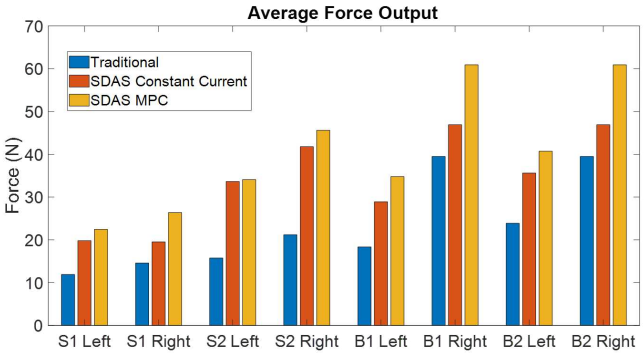

Figure 5: Average force output of all 60 contractions for each stimulation protocol among each participant

$d_f(x, y)$. To track displacement over a full contraction, we accumulate the displacement with respect to the first image of the motion. The accumulated displacement at frame i, defined as $s_i(x, y) = (x_i, y_i,) - (x_0, y_0)$ where $(x_i, y_i) = (x_{i-1}, y_{i-1}) + d_f(x, y)$. Once the displacement is accumulated for all images, the strain is computed by applying a Savitszky-Golay [55] on the cumulative displacement in axial direction as it is expected the quadriceps expand axially during isometric contractions.

B. Correlation Between Muscle Contractility of the VL *and* VM *and Hill-Huxley Model Dynamics*

Based on (2), the scaling factor that drives the force generated by each electrode has a force-driven component driven by $\alpha_p F_{pj}$ and a recovery-driven component in $\frac{A_p - A_{p0}}{\tau_{fp}}$, which is driven by the time constant τ_{fp}. Since, the dynamics for A_p are driven by $\alpha_p F_{pj}$, we explored if the US imaging can be used to update the dynamics of A based on real-time muscle contractility information based on results from [49] which shows a correlation in strain measures from US images and force output of the quadriceps. Essentially, from an imaging perspective as the force produced by the muscle decreases, the muscle contractility also follows a similar trend. The US imaging-derived strain measures, which are gradient of accumulated muscle displacement during a contraction, quantify the change in muscle contractility due to the FES-induced fatigue.

To test this hypothesis, we collected US plane wave images of the *VL* and *VM* on each leg while the SDAS protocol was administered to both muscles simultaneously. An ultrasound transducer (L7.0SC Prodigy Probe, S-Sharp, Taiwan) was placed on the thigh to obtain transverse images of the quadriceps to identify the structures and location of the *VM* and *VL* in relation to the thigh. The location was determined

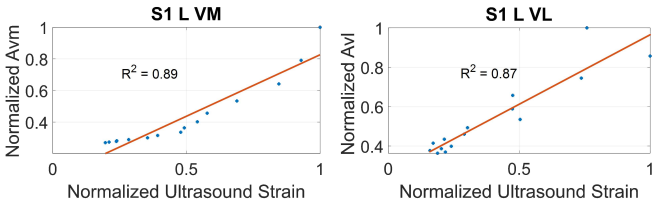

Figure 6: Normalized A for both the *VL* and *VM* of the left leg of participant S1 compared to the normalized strain values from US during SDAS.

by visualizing the muscle response to a 1 second stimulation pulse. Once the muscle was located, the transducer was rotated to a longitudinal view of the muscle. The fatiguing protocol was then conducted and ultrasound images during every 4th contraction were collected at 1000 Hz. The procedure was repeated to obtain images of both muscles (*VM* and *VL*) and both legs of each participant. Since the muscle fatigues after the two minute protocol, images of the *VL* and *VM* were collected on different days. The strain during each contraction was measured using the adaptive speckle tracking algorithm in [49]. The experimental setup to collect US images during SDAS is shown in Fig. 1. To test our hypothesis that US can be used to update $A_p$for both the *VL* and *VM* during SDAS, we computed strain measurements from US-images of the *VL* and *VM* collected during the fatiguing protocol. A representative strain result from the *VL* and *VM* of the left leg of participant B2 is shown in Fig. 7A. Fig. 7B further shows the average accumulated strain map at the end of each imaged contraction for the left leg of each participant. It is seen that the strain decays along with the contraction number. Fig. 8 shows the average strain determined from the US images collected of the *VL* and *VM*. The average strain of the first three contractions (pre-fatigue) and final three contractions (post-fatigue) is 0.49 ± 0.13 and 0.12 ± 0.09 for the *VL* and 0.50 ± 0.23 and 0.17 ± 0.09 for the *VM* .

A one-tailed t-test showed that the strain values during pre and post fatigued states were significantly different for both the *VL* and *VM* ($p < 0.001$and $p = 0.004$, respectively). These results are consistent with the results in [49],which also determined a statistically significant difference in strain of the *Vastus Intermedius* (*VI*) during pre and post fatigue states for a traditional stimulation approach.

We further compared the US-derived strain measurements with changes in dynamics of A_{vl} and A_{vm} based on identified model parameters. Fig. 6 shows the normalized ultrasound strain compared to the respective normalized value of A_p for both the *VL* and *VL* for participant A1. The average R^2 value between normalized A and normalized US-derived strain measurements was 0.88 ± 0.06 for both the VL and VM on all participants indicating a strong correlation between A and US-derived strain changes.

V. SDAS Walking with a Hybrid Exoskeleton: Proof of Concept Demonstration

The goal of this section is to evaluate the feasibility of adapting the isometric SDAS muscle to be used in conjunction with a powered exoskeleton. In our previous work [51], we used an MPC approach for traditional FES to track a swing phase knee trajectory during a walking task while incorporating real-time US imaging measurements to update a fatigue model. In this section, we used an MPC controller for SDAS to track a swing phase trajectory with real-time US imaging measurements from one of the quadriceps muscle regions. The MPC uses SDAS model dynamics rather than traditional knee extension dynamics. When adding an electric motor, the swing phase in (9) dynamics become

$$J\ddot{\theta} + T_p(\theta, \dot{\theta}) + G(\theta) = \tau_{stim} + \tau_m \quad (12)$$

$$= F_{stim} l + \tau_m \quad (13)$$

where τ_m is the torque from the motor, l is the shank length and F_{stim} is defined by the model in 2-8

A. Obtaining Real-Time Fatigue Measures from Ultrasound Images

In our previous study [50], [51], we adapted the speckle tracking algorithm for real-time performance with a hybrid exoskeleton. To achieve this real-time adaptation, we note that the computation time of the normalized cross-correlation increases quadratically with the size of the kernel, search window, and ROI. In addition, there is an interpolation step necessary to estimate small tissue motion between sets of US images which increases the number of spatial locations at which the correlation coefficient is computed. To overcome these challenges we leverage the fact that $\gamma(x, y)$ does not depend on γ at any other position and use a parallel processing framework as shown in Fig. 9. The GPU frameworks reduces the computation time of strain between two consecutive images from the scale of minutes to <1 second. It is of note that to obtain a fatigue measurement for a complete contraction, the displacement is accumulating thus to total time for a measurement is the time between two frames multiplied by the number of frames in the contraction. The strain imaging algorithm presented in this study along with our previous studies [48], [49] analyzed US images during isometric contractions. To mimic this condition in a real-time exoskeleton walking environment, we design a diagnostic stimulation protocol which consists of a one-second diagnostic pulse applied at a point during the desired walking trajectory at which the knee joint had zero velocity. During the diagnostic pulse, the US system was triggered to collect raw US images and transfer it to the GPU platform for computation.

B. Non-Isometric Parameter Identification

The model in (9) depends on parameters $\bar{\vartheta}, \lambda_1, \lambda_2$ and A_{p40}. To identify these parameters, in session 5, we performed a set of system identification experiments in which a participant was seated in the dynamometer. First, A_{p40} was identified using the same procedure in section was identified using the same procedure in section III-B for A_p with the knee joint was held at 40 degrees instead of at 0 degrees from the vertical. A_{p40} was estimated by solving the optimization problem described in (10), while the other parameters were

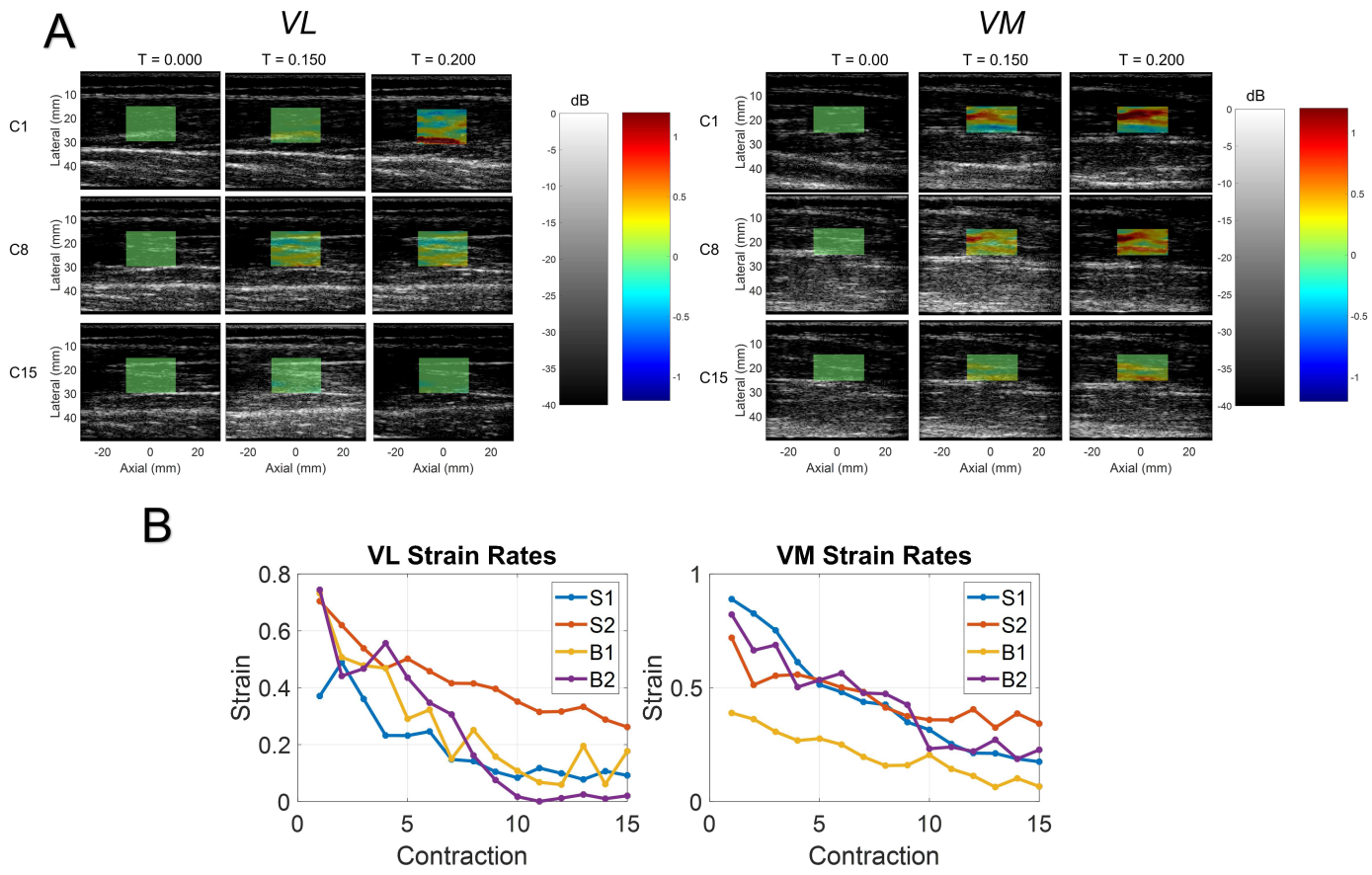

Figure 7: (A) Representative strain maps of the *VL* and *VM* at chosen time points during the 1st, 8th and 15th contraction of the SDAS fatiguing protocol on the left leg of all participants (B) Strain rates of the *VL* and *VM* of the left leg of all participants during SDAS. The strain at each contraction was calculated by taking the average of the accumulated strain map at the end of the contraction.

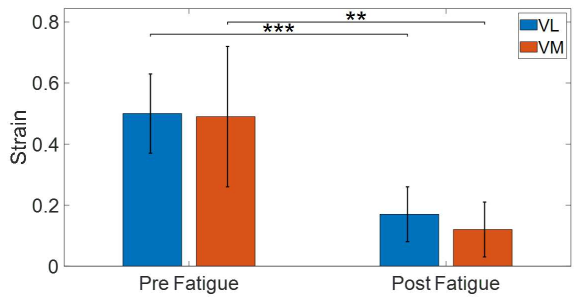

Figure 8: Average strain across the first three (pre) and last three (post) imaged contractions for all participants with standard deviation. A one-tailed t-test revealed a significant difference in strain between pre and post fatigue states for both the *VL* and *VM*.

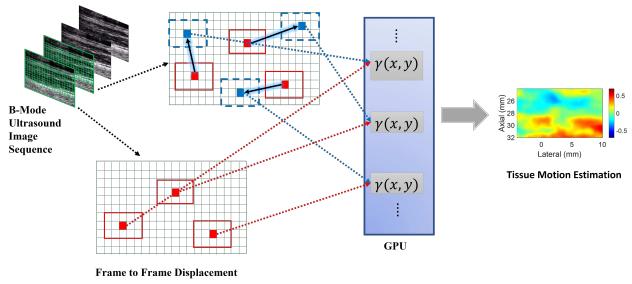

Figure 9: Parallel computation of an adaptive speckle tracking algorithm to measure real-time strain changes. The displacements at each point in the region of interest (ROI, green squares) between two US images are independent and can be computed simultaneously. US images are loaded onto the GPU, and the tissue motion at each point is computed using in parallel NVIDIA's CUDA architecture. The solid red squares highlight original tracking points with solid lines indicating the surrounding kernels in the original frame, while the blue squares represent the displaced points in the tracking frame. Red highlights a positive strain (i.e., tension), while blue represents a negative strain (i.e., compression) in the direction of propagation of US.

the same as those identified when the knee angle was held at 90 degrees. Next, to identify $\bar{\vartheta}, \lambda_1$, and λ_2, we stimulated the participant's quadriceps using the SDAS protocol in the isokinetic mode of the dynamometer. This allowed the knee joint to move freely upon stimulation. The stimulation current and timing was varied for multiple cycles to ensure the model

was accurate for a wide range of knee joint velocities. The parameters for $\bar{\vartheta}, \lambda_1$, and λ_2 were determining by solving the optimization problem

$$\min J = \frac{1}{n}\sum_{i=1}^{n}(\theta_{1p}(i,u) - \theta_{1m})^2 + \frac{1}{n}\sum_{i=1}^{n}(\theta_{4p}(i,u) - \theta_{4m})^2$$

where $\theta_{1p}(i,u), \theta_{1m}$ are the predicted and measured knee joint position during the first cycle and $\theta_{4p}(i,u), \theta_{4m}$ are the predicted and measured knee joint position during the fourth cycle. The estimated parameters were used in (9) to predict the force during the second and third cycles as model validation.

C. MPC of SDAS and a Hybrid Exoskeleton During a Knee Extension Task

To perform a control task to track the swing phase trajectory we used an MPC scheme that solves the following optimal control problem

$$\begin{gathered}\min_{\boldsymbol{u}} J = \int_0^T l(x,u) \\ s.t: J\ddot{\theta} + G(\theta) + \tau_p = T_{stim} l + u_5 \\ \frac{dF_j}{dt} = [\bar{G}_p(\theta)\dot{\theta} + A(\theta)][A_p \frac{\bar{C}_{N_{pj}}}{K_{mp}+\bar{C}_{N_{pj}}} - \frac{F_{pj}}{\tau_{1p}+\tau_{2p}\frac{\bar{C}_{Np_j}}{K_{mp}+\bar{C}_{N_{pj}}}}] \\ 0 \le u_{j=1,2,3,4} \le 1 \\ \underline{u}_5 \le u_5 \le \bar{u}_5 \end{gathered} \tag{14}$$

where the states $x \in \mathbb{R}^8$ and controls $u \in \mathbb{R}^5$ are defined as $x = \begin{bmatrix} F_{vm1} & F_{vm2} & A_{vm} & F_{vl1} & F_{vl2} & A_{vl} & \theta & \dot{\theta} \end{bmatrix}^T$ and $u = \begin{bmatrix} u_1 & u_2 & u_3 & u_4 & u_5 \end{bmatrix}^T$ where u_{1-4} are normalized stimulation intensities at each electrode and u_5 is the motor input. The cost function is defined as

$$l(x,u) = (x - x_d(t))^T Q (x - x_d(t)) + u^T R u$$

where $x_d(t) \in \mathbb{R}^8$ represents the desired states. In this application the control objective is to tracking a desired position and velocity, and further ensuring that the dynamics for A_{vm} and A_{vl} do not decay to quickly. To achieve this, the desired trajectory of $A_{vl}$and A_{vm} were set to A_{p40} for each muscle respectively and the desired forces and the respective weights were set to zero. To ensure the MPC scheme did not rely only on motor, a large penalty was placed on the motor input u_5.

D. Experiments using a Hybrid Exoskeleton

Similar to our previous study [51] which looked at real-time US imaging of the VI to optimize shared control using the traditional approach, two participants with SCI and one participant without disability donned an INDEGO (Ekso Bionics, USA) exoskeleton embedded with FES capabilities and performed two trials consisting of 20 steps (10 left, 10 right). During each trial, MPC framework was used to track the left knee trajectory during the swing phase of the gait cycle. A linear transducer (L7.0SC Prodigy Probe, S-Sharp, Taiwan) connected to an imaging platform equipped with a GPU (NVIDIA Titan V) was placed on the quadriceps to image the VM and was secured using medical tape. At the beginning of each trial, real-time US measurements were collected to initialize the dynamics of A_{vm} for the subsequent trial. Additionally, the participant started each trial in a seated position and performed a sit-to-stand task solely using a feedback controller before performing the walking. The trajectories for the sit-to-stand task were designed based on a virtual constraint method in [56].

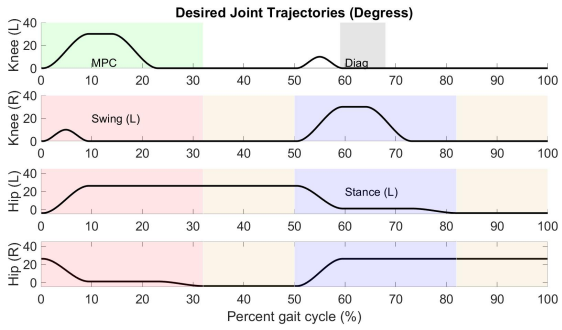

Figure 10: Joint trajectories during each gait cycle to perform a walking motion. The MPC framework was used to control swing phase dynamics on the left leg and a feedback controller was used on all other joints.

The timing and control of the exoskeleton was governed by a finite state machine (FSM) with four states: initial sit-to-stand, right half step, left step, and right step. The FSM started by transitioning from sit-to-stand followed by a right half step, and it proceeded to alternate between left step and right step for the entire 10 left step trial. Both step states in the FSM were divided into the following three sub-states: swing leg hip and knee flexion along with stance leg flexion/extension, swing leg knee extension, and stance leg hip extension. The trajectory for each sub-state was designed using a third order polynomial trajectory based on the desired angles of hip and knee flexion and extension. The desired flexion and extension angles for the hip and knee are highlighted in Fig. 10. The MPC algorithm was implemented on the left knee during states 2-5 of the FSM to control swing phase dynamics while the right knee and both hips were controlled by a robust-integral-signum-error (RISE) controller [57]. The RISE controller,$\tau \in \mathbb{R}$ is given by the control law

$$\tau = k_1 e_2 + \int_0^t [k\alpha_2 + \beta sgn(e_2)]dt$$

with tracking errors $e_1 \in \mathbb{R}, e_2 \in \mathbb{R}$ defined as

$$\begin{aligned} e_1 &= \theta_d - \theta \\ e_2 &= \dot{e}_1 + \alpha_1 e_1 \end{aligned}$$

where $k_1, \alpha_1, \alpha_2, \beta \in \mathbb{R}^+$ are positive gains, $\theta_d(t) \in \mathbb{R}$ is the desired trajectory, $\theta(t) \in \mathbb{R}$ is the joint angle and $sgn()$ is a signum function. US imaging-based fatigue measurements were received during each left step based on images collected during a diagnostic pulse to provide a quasi-isometric contraction while the left leg was in the stance phase. The periods during which the quadriceps were stimulated by the MPC and by a diagnostic FES pulse are seen in Fig. 10. and an overview of the hybrid exoskeleton-FES system is shown in Fig. 11

Once parameters, were identified, the MPC framework in (14) was implemented to control the swing phase during a

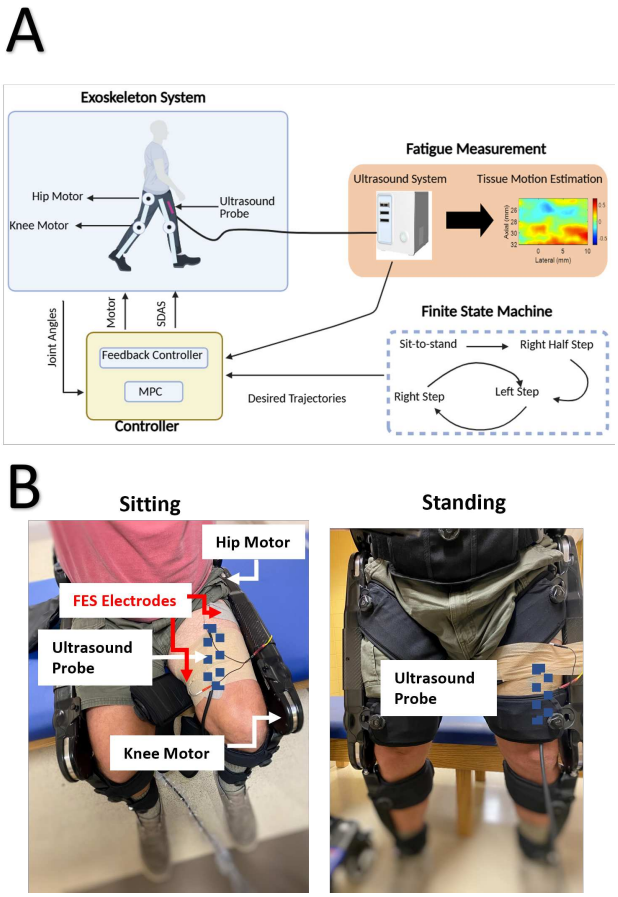

Figure 11: (A) Overview of the hybrid exoskeleton system with SDAS. Real-time fatigue measurements are used to allocate inputs between SDAS and motor. (B) Highlight of the experimental setup on one participant with SCI during the traditional MPC approach. The SDAS approach deploys the same framework form the INDEGO exoskeleton while using the SDAS MPC approach presented in (14) .

walking task. Real-time US-derived strain measurements of the VM were collected during the left leg stance phase and a strain measurement was calculated using a parallel processing framework in [50]. The normalized strain measurement was computed in real time using a GPU-based parallel computation scheme described in [50], [51] and used to update the model of A_{vm}in (2) while A_{vl} was obtained using the model only due to computational resources of collecting US images from multiple probes at the same time.

The average foot position during both trials for participant with SCI S1 when the MPC framework in (14) was usedto control the swing phase dynamics is shown in Fig. 13along with foot position trajectories in both directions whenusing a MPC framework in our previous studies [51], [58] tocontrol a hybrid exoskeleton using the traditional stimulationapproach. It is clear that the shared control framework usingboth stimulation approaches results in similar foot position. Toanalyze the effect of using SDAS compared to the traditional

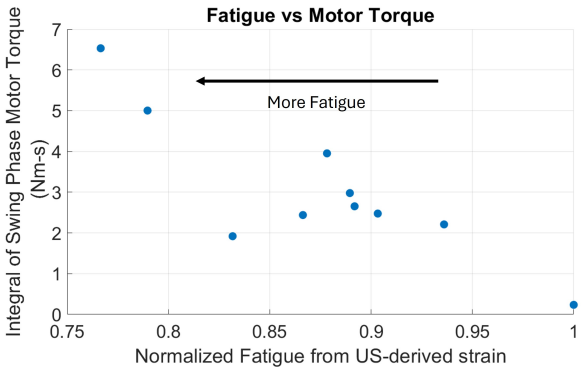

Figure 12: Integral of motor torque compared to normalized fatigue value from ultrasound imaging for steps 1-10 of participant S1. A normalized fatigue value of 1 indicates the muscle is not fatigued and smaller fatigue values indicate higher fatigue levels.

approach, we looked at the motor effort by the MPC scheme during the swing phase of each step when using traditional FES protocols versus SDAS. Fig. 14 shows the representative integral of motor input during steps 1-10 for participant S1 in both cases along with a linear trend. In both cases, as step number increases, the muscle begins to fatigue and the motor torque increases . The average integral of motor torque over two trials (20 steps) was 24.12 ± 11.82 and 2.78 ± 1.50 Nm-s, respectively. Similarly, for participant S2 the average integral of motor torques during the traditional MPC and SDAS approach were 45.41 ± 14.53 and 30.94 ± 6.03 respectively and the integrals of motor torque were 16.53 ± 1.87 and 11.68 ± 1.73 for the participant with no disability. A one-tailed t-test was performed to show statistical significance at a 95% confidence level ($p < 0.001$) for all three participants as highlighted in Fig. 15 indicating that the SDAS approach results in a lower amount of motor assistance. Fig. shows the integral of motor torque for participant with S1 with respect to the ultrasound-derived fatigue measurement highlighting that as the *VM* fatigues, the amount of motor assistance increases. Finally, for participant S1, we also collected real-time ultrasound measures of the VM at the end of each trial to assess the fatigue of the muscle, and the fatigue index was 0.84 after trial 1 and 0.79 after trial 2. Since the kinematics remain unchanged, the decreased torque from the motor when using SDAS compared to the traditional approach indicates that more power is being generated by FES. Further, this increase in power generation did not increase the fatigue rate of the VM as seen by the fatigue measures from ultrasound.

VI. Discussion

The results presented in this study demonstrate the potential of utilizing US-derived strain measurements of the *VL* and *VM* in closed-loop control during SDAS. We first proposed a modified model that includes stimulation intensity and frequency in SDAS. The proposed model calculates the individual force generated by each stimulated electrode during SDAS as well as the total force generation as a sum of individual forces. The model also accounts for stimulation intensity by scaling

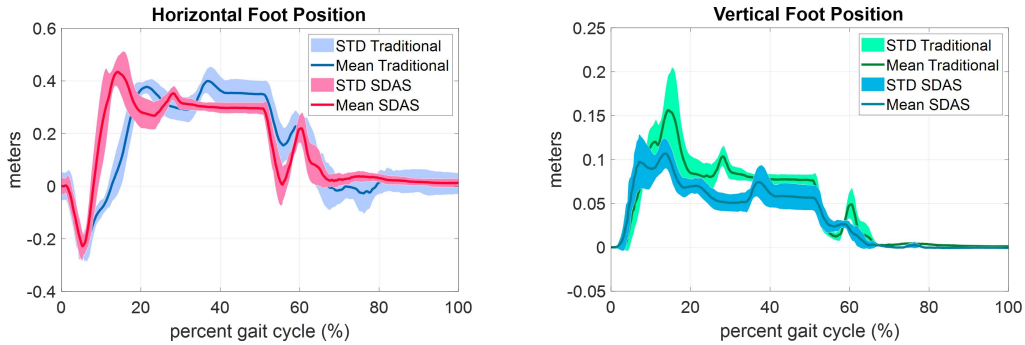

Figure 13: Horizontal and vertical foot position when the MPC framework for shared control with SDAS was implemented participant S1 with SCI compared to the foot position when MPC with the traditional stimulation approach was implemented.

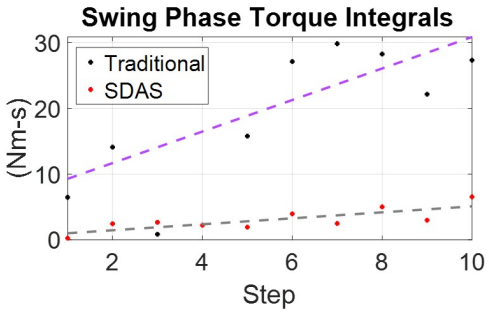

Figure 14: Integrals of swing phase motor torques for participant S1 with SCI during steps 1-10 when using shared control with traditional FES compared to SDAS.

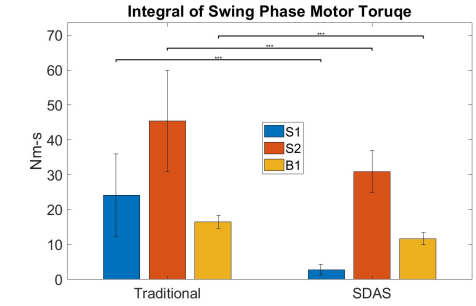

Figure 15: Average torque integral (Nm-s) during the swing phase over 20 steps (2 trials) when using shared control with the traditional stimulation approach compared to SDAS.

the calcium dynamics by a normalized intensity between a saturation and threshold. That is, if a person is stimulated at their maximum intensity, the scaled calcium dynamics in (3) will be the same as the calcium dynamics in [52].

We then validated parameters obtained from system identification by comparing the predicted force when both muscles were stimulated during SDAS to the measured force during a SDAS protocol as seen in Fig. 3. The high R^2 value indicates that the proposed model is effective at correlating the force dynamics of both the *VL* and *VM*. However, we note that there is still a minor difference between measured and predicted forces.The average RMSE between measured and predicted forces are 7.27 ± 2.43 Newtons and could be associated with minor changes in electrode placement and muscle composition between each visit. These changes in electrode placement and muscle composition between each visit will impact the identified parameters in the model which now act as estimates rather than true parameters. This will impact the MPC strategy as the optimization problem in (14) requires exact model knowledge. While in this manuscript we used an MPC approach which relies on the exact dynamics as a constraint in the optimization, our group has investigated robust MPC approaches to deal with model approximation errors, which could be caused day-to-day physiological changes or electrode placement errors [27]. Electrode placements can be improved through motor point identification [6], though tedious and impractical for daily use, can standardize electrode placement. Other approaches such as a larger electrode array and automatic electrode identification [59] may be used to improve electrode placement.

We also investigated the use of US-derived strain measures in the proposed model to analyze and measure fatigue rates of both the *VL* and *VM* individually.. This benefit of US-derived measures has an advantage over the dynamometer, which can only provide the net output of both muscles and is unclear how to decompose their each muscle contributions and fatigue rates. Thus, we look at changes in the dynamics of A_{vm} and A_{vl} in (2) and how they relate to the changes in strain from US images. As seen in Fig. 6, there is a high R^2 value when correlating normalized strain and normalized A dynamics. This indicates that US-imaging can potentially be used as a sensing modality of fatigue state to inform closed-loop SDAS. Additionally, we incorporated the model into an MPC approach to modulate current intensities to track a desired force. Simulation results showed that initially, the desired and actual force matched until the muscle began to fatigue. To validate the simulation results, we applied the optimized inputs during SDAS experimentally and compared the force output and fatigue rates to the constant current SDAS and traditional approach. Results showed that using optimized inputs results in the highest average power and lower power decay. Further, the RMSE between the measured total force from optimized inputs and the force from the simulations was less that 10 Newtons for all participants.

The results in this study are consistent with previous studies that showed improved fatigue resistance and power output of SDAS compared to a traditional stimulation approach [13]–

[15]. Similarly, the statistically significant decay in muscle contractility of the *VL* and *VM* shown in Fig. 8 is consistent with our previously published work [48]. We further validated the nonisometric SDAS dynamic model and showed, for the first time, its application in a hybrid exoskeleton to perform a walking task. Compared to the previous walking results with real-time US feedback in [51], the motor effort required when using SDAS was significantly lower. Since the total torque required to perform a walking task remained the same in each case, the lower motor effort during SDAS indicates that more power is being generated by FES while the functional foot clearance in both the horizontal and vertical direction remain consistent.

From a modeling and control perspective, one of the challenges with the proposed approach is the dependence of exact model knowledge. In this manuscript, we obtain model parameters by performing a system identification procedure which could become cumbersome for implementation in a clinical setting. Further, the ability to scale the number of SDAS electrodes on each muscle presents a challenge. In the proposed model, the number of electrodes can be scaled for each muscle by summing the force generated from each electrode at the specific muscle as seen in 5. However, this process increases the number of states and inputs in the MPC problem setup which could potentially have an impact on the optimization performance. This challenge could be addressed with either increasing the hardware power and CPU/GPU requirements to perform complex optimizations or developing data-driven and dimension reduction based control approaches, some of which has been investigated by our group for ankle joint control using exoskeleton and FES [60], [61]. In the future we look to expand these approaches for closed-loop SDAS control.

In terms of clinical use perspective and full scale implementation perspective, this study has limitations with respect to 1) sample size of SDAS walking participants 2) extensive imaging setup 3) computation and hardware resources required to image multiple muscles simultaneously. In terms of sample size, the SDAS walking scheme in this manuscript is a proof of concept and demonstrated on one participant with SCI over 20 walking steps. Further experiments can expand the work in this study to show performance over longer duration and with multiple participants. In reference to computation and hardware resources, as mentioned in our previous study [51], there is a tradeoff between US computation time and fatigue measurement accuracy for real-time implementation. Adapting certain parameters of our speckle tracking algorithm such as the kernel or search window and using a larger region of interest will result in more accurate fatigue measurements however relaxing these parameters will result in faster performance for real-time implementation. The US imaging setup during walking experiments is critical as we aim to image specific muscles during a dynamic condition compared to our previous work that focused on seated isometric conditions. During the walking experiments, we have to ensure that the probe does not shift from the position which images the muscle. This is currently done using a 3D printed ultrasound transducer holder along with medical tape. However in the future body-conformable US imaging sensors that are easy to attach to the leg and are less prone to dislocations could be developed. Wearable ultrasound transducers, shown in studies like [62] and [63], are already developed and validated. These smaller US transducers could reduce the computational and hardware limitations of our current setup while simultaneously obtaining information from multiple muscles.

VII. Conclusion

In this work, we propose a phenomenological model that can predict the force generated at each electrode during SDAS. The model can account for phase delayed stimulation frequency and intensity. We further investigated the muscle contractility of the VL and VM during SDAS with the aim of incorporating US images into the model. Analysis of US imaging-derived strain rates of both muscles indicated changes in muscle contractility between pre and post-fatigue states has a strong correlation with the proposed dynamic model's fatigue variable. Additionally, MPC simulations and experimental validation show that using optimized current inputs during a fatiguing protocol increases muscle force output and the fatigue decay rate. The SDAS approach was then extended to a non-isometric dynamic model and incorporated into a shared control framework in a hybrid exoskeleton. Preliminary experiments showed the functionality of walking with SDAS and demonstrated that the overall effort required from the motor was reduced when compared to the traditional stimulation approach, implying that more power was being generated by SDAS.

References

[1] O. A. Howlett, N. A. Lannin, L. Ada, and C. McKinstry, "Functional electrical stimulation improves activity after stroke: a systematic review with meta-analysis," *Archives of physical medicine and rehabilitation*, vol. 96, no. 5, pp. 934–943, 2015.

[2] A. Kralj and T. Bajd, *Functional electrical stimulation: standing and walking after spinal cord injury*. Routledge, 2022.

[3] T. M. Kesar, R. Perumal, D. S. Reisman, A. Jancosko, K. S. Rudolph, J. S. Higginson, and S. A. Binder-Macleod, "Functional electrical stimulation of ankle plantarflexor and dorsiflexor muscles: effects on poststroke gait," *Stroke*, vol. 40, no. 12, pp. 3821–3827, 2009.

[4] B. D. Doll, N. A. Kirsch, X. Bao, B. E. Dicianno, and N. Sharma, "Dynamic optimization of stimulation frequency to reduce isometric muscle fatigue using a modified hill-huxley model," *Muscle & nerve*, vol. 57, no. 4, pp. 634–641, 2018.

[5] A. Botter, G. Oprandi, F. Lanfranco, S. Allasia, N. A. Maffiuletti, and M. A. Minetto, "Atlas of the muscle motor points for the lower limb: implications for electrical stimulation procedures and electrode positioning," *European journal of applied physiology*, vol. 111, pp. 2461–2471, 2011.

[6] M. Gobbo, N. A. Maffiuletti, C. Orizio, and M. A. Minetto, "Muscle motor point identification is essential for optimizing neuromuscular electrical stimulation use," *Journal of neuroengineering and rehabilitation*, vol. 11, no. 1, pp. 1–6, 2014.

[7] A. S. Gorgey, C. D. Black, C. P. Elder, and G. A. Dudley, "Effects of electrical stimulation parameters on fatigue in skeletal muscle," *journal of orthopaedic & sports physical therapy*, vol. 39, no. 9, pp. 684–692, 2009.

[8] G. Deley, D. Laroche, and N. Babault, "Effects of electrical stimulation pattern on quadriceps force production and fatigue," *Muscle & nerve*, vol. 49, no. 5, pp. 760–763, 2014.

[9] B. Dreibati, C. Lavet, A. Pinti, and G. Poumarat, "Influence of electrical stimulation frequency on skeletal muscle force and fatigue," *Annals of physical and rehabilitation medicine*, vol. 53, no. 4, pp. 266–277, 2010.

[10] A. S. Gorgey, H. J. Poarch, D. R. Dolbow, T. Castillo, and D. R. Gater, "Effect of adjusting pulse durations of functional electrical stimulation cycling on energy expenditure and fatigue after spinal cord injury." *Journal of Rehabilitation Research & Development*, vol. 51, no. 9, 2014.

[11] Y.-J. Chang and R. K. Shields, "Doublet electrical stimulation enhances torque production in people with spinal cord injury," *Neurorehabilitation and neural repair*, vol. 25, no. 5, pp. 423–432, 2011.

[12] V. Nekoukar, "Control of functional electrical stimulation systems using simultaneous pulse width, amplitude, and frequency modulations," *Neuromodulation: Technology at the Neural Interface*, vol. 24, no. 8, pp. 1467–1474, 2021.

[13] R. J. Downey, M. J. Bellman, H. Kawai, C. M. Gregory, and W. E. Dixon, "Comparing the induced muscle fatigue between asynchronous and synchronous electrical stimulation in able-bodied and spinal cord injured populations," *IEEE Transactions on Neural Systems and Rehabilitation Engineering*, vol. 23, no. 6, pp. 964–972, 2014.

[14] N. M. Malešević, L. Z. Popović, L. Schwirtlich, and D. B. Popović, "Distributed low-frequency functional electrical stimulation delays muscle fatigue compared to conventional stimulation," *Muscle & nerve*, vol. 42, no. 4, pp. 556–562, 2010.

[15] M. Laubacher, A. E. Aksöz, R. Riener, S. Binder-Macleod, and K. J. Hunt, "Power output and fatigue properties using spatially distributed sequential stimulation in a dynamic knee extension task," *European journal of applied physiology*, vol. 117, pp. 1787–1798, 2017.

[16] D. G. Sayenko, R. Nguyen, M. R. Popovic, and K. Masani, "Reducing muscle fatigue during transcutaneous neuromuscular electrical stimulation by spatially and sequentially distributing electrical stimulation sources," *European journal of applied physiology*, vol. 114, pp. 793–804, 2014.

[17] D. G. Sayenko, R. Nguyen, T. Hirabayashi, M. R. Popovic, and K. Masani, "Method to reduce muscle fatigue during transcutaneous neuromuscular electrical stimulation in major knee and ankle muscle groups," *Neurorehabilitation and neural repair*, vol. 29, no. 8, pp. 722–733, 2015.

[18] A. J. Bergquist, V. Babbar, S. Ali, M. R. Popovic, and K. Masani, "Fatigue reduction during aggregated and distributed sequential stimulation," *Muscle & nerve*, vol. 56, no. 2, pp. 271–281, 2017.

[19] G. Ye, P. Theventhiran, and K. Masani, "Effect of spatially distributed sequential stimulation on fatigue in functional electrical stimulation rowing," *IEEE Transactions on Neural Systems and Rehabilitation Engineering*, vol. 30, pp. 999–1008, 2022.

[20] E. Jafari, P. Kajganic, V. Bergeron, J. Di Marco, A. Metani, and L. Popovic-Maneski, "Efficacy of high-versus moderate-intensity spatially distributed sequential stimulation in subjects with spinal cord injury: an isometric study," *Journal of NeuroEngineering and Rehabilitation*, vol. 22, no. 1, p. 65, 2025.

[21] A. J. Del-Ama, A. D. Koutsou, J. C. Moreno, A. De-Los-Reyes, Á. Gil-Agudo, and J. L. Pons, "Review of hybrid exoskeletons to restore gait following spinal cord injury." *Journal of Rehabilitation Research & Development*, vol. 49, no. 4, 2012.

[22] A. J. Del-Ama, Á. Gil-Agudo, J. L. Pons, and J. C. Moreno, "Hybrid fes-robot cooperative control of ambulatory gait rehabilitation exoskeleton," *Journal of neuroengineering and rehabilitation*, vol. 11, pp. 1–15, 2014.

[23] K. H. Ha, H. A. Quintero, R. J. Farris, and M. Goldfarb, "Enhancing stance phase propulsion during level walking by combining fes with a powered exoskeleton for persons with paraplegia," in *2012 Annual International Conference of the IEEE Engineering in Medicine and Biology Society*. IEEE, 2012, pp. 344–347.

[24] K. H. Ha, S. A. Murray, and M. Goldfarb, "An approach for the cooperative control of fes with a powered exoskeleton during level walking for persons with paraplegia," *IEEE Transactions on Neural Systems and Rehabilitation Engineering*, vol. 24, no. 4, pp. 455–466, 2015.

[25] M. A. Alouane, W. Huo, H. Rifai, Y. Amirat, and S. Mohammed, "Hybrid FES-exoskeleton controller to assist sit-to-stand movement," *IFAC-PapersOnLine*, vol. 51, no. 34, pp. 296–301, 2019.

[26] X. Bao, Z. Sheng, B. E. Dicianno, and N. Sharma, "A tube-based model predictive control method to regulate a knee joint with functional electrical stimulation and electric motor assist," *IEEE Transactions on Control Systems Technology*, vol. 29, no. 5, pp. 2180–2191, 2020.

[27] Z. Sun, A. Iyer, K. Lambeth, C. Cleveland, and N. Sharma, "Knee extension tracking and fatigue regulation results using a robust mpc approach in a hybrid exoskeleton," *Control Engineering Practice*, vol. 141, p. 105717, 2023.

[28] N. A. Kirsch, X. Bao, N. A. Alibeji, B. E. Dicianno, and N. Sharma, "Model-based dynamic control allocation in a hybrid neuroprosthesis," *IEEE Transactions on Neural Systems and Rehabilitation Engineering*, vol. 26, no. 1, pp. 224–232, 2017.

[29] Z. Sheng, Z. Sun, V. Molazadeh, and N. Sharma, "Switched control of an n-degree-of-freedom input delayed wearable robotic system," *Automatica*, vol. 125, p. 109455, 2021.

[30] M. Laubacher, E. A. Aksoez, A. K. Brust, M. Baumberger, R. Riener, S. Binder-Macleod, and K. J. Hunt, "Stimulation of paralysed quadriceps muscles with sequentially and spatially distributed electrodes during dynamic knee extension," *Journal of neuroengineering and rehabilitation*, vol. 16, pp. 1–12, 2019.

[31] R. S. Baptista, M. CC Moreira, L. DM Pinheiro, T. R. Pereira, G. G. Carmona, J. PD Freire, J. AI Bastos, and A. Padilha Lanari Bo, "User-centered design and spatially-distributed sequential electrical stimulation in cycling for individuals with paraplegia," *Journal of NeuroEngineering and Rehabilitation*, vol. 19, no. 1, p. 45, 2022.

[32] R. J. Downey, T.-H. Cheng, M. J. Bellman, and W. E. Dixon, "Closed-loop asynchronous neuromuscular electrical stimulation prolongs functional movements in the lower body," *IEEE Transactions on neural systems and rehabilitation engineering*, vol. 23, no. 6, pp. 1117–1127, 2015.

[33] N. K. Vøllestad, "Measurement of human muscle fatigue," *Journal of neuroscience methods*, vol. 74, no. 2, pp. 219–227, 1997.

[34] D. R. Rogers and D. T. MacIsaac, "Emg-based muscle fatigue assessment during dynamic contractions using principal component analysis," *Journal of Electromyography and Kinesiology*, vol. 21, no. 5, pp. 811–818, 2011.

[35] M. Cifrek, V. Medved, S. Tonković, and S. Ostojić, "Surface emg based muscle fatigue evaluation in biomechanics," *Clinical biomechanics*, vol. 24, no. 4, pp. 327–340, 2009.

[36] A. Georgakis, L. K. Stergioulas, and G. Giakas, "Fatigue analysis of the surface emg signal in isometric constant force contractions using the averaged instantaneous frequency," *IEEE transactions on biomedical engineering*, vol. 50, no. 2, pp. 262–265, 2003.

[37] F. Mandrile, D. Farina, M. Pozzo, and R. Merletti, "Stimulation artifact in surface emg signal: effect of the stimulation waveform, detection system, and current amplitude using hybrid stimulation technique," *IEEE Transactions on neural systems and rehabilitation engineering*, vol. 11, no. 4, pp. 407–415, 2003.

[38] R. S. Witte, K. Kim, B. J. Martin, and M. O'Donnell, "Effect of fatigue on muscle elasticity in the human forearm using ultrasound strain imaging," in *2006 International Conference of the IEEE Engineering in Medicine and Biology Society*. IEEE, 2006, pp. 4490–4493.

[39] K. Bouillard, A. Nordez, and F. Hug, "Estimation of individual muscle force using elastography," *PloS one*, vol. 6, no. 12, p. e29261, 2011.

[40] P. Andonian, M. Viallon, C. Le Goff, C. de Bourguignon, C. Tourel, J. Morel, G. Giardini, L. Gergele, G. P. Millet, and P. Croisille, "Shear-wave elastography assessments of quadriceps stiffness changes prior to, during and after prolonged exercise: a longitudinal study during an extreme mountain ultra-marathon," *PLoS One*, vol. 11, no. 8, p. e0161855, 2016.

[41] J. A. Hides, C. A. Richardson, and G. A. Jull, "Use of real-time ultrasound imaging for feedback in rehabilitation," *Manual therapy*, vol. 3, no. 3, pp. 125–131, 1998.

[42] J. Heckmatt, N. Pier, and V. Dubowitz, "Real-time ultrasound imaging of muscles," *Muscle & Nerve: Official Journal of the American Association of Electrodiagnostic Medicine*, vol. 11, no. 1, pp. 56–65, 1988.

[43] P. Hodges, L. Pengel, R. Herbert, and S. Gandevia, "Measurement of muscle contraction with ultrasound imaging," *Muscle & Nerve: Official Journal of the American Association of Electrodiagnostic Medicine*, vol. 27, no. 6, pp. 682–692, 2003.

[44] C. Castellini, G. Passig, and E. Zarka, "Using ultrasound images of the forearm to predict finger positions," *IEEE Transactions on Neural Systems and Rehabilitation Engineering*, vol. 20, no. 6, pp. 788–797, 2012.

[45] S. Sikdar, H. Rangwala, E. B. Eastlake, I. A. Hunt, A. J. Nelson, J. Devanathan, A. Shin, and J. J. Pancrazio, "Novel method for predicting dexterous individual finger movements by imaging muscle activity using a wearable ultrasonic system," *IEEE Transactions on Neural Systems and Rehabilitation Engineering*, vol. 22, no. 1, pp. 69–76, 2013.

[46] N. Akhlaghi, C. A. Baker, M. Lahlou, H. Zafar, K. G. Murthy, H. S. Rangwala, J. Kosecka, W. M. Joiner, J. J. Pancrazio, and S. Sikdar, "Real-time classification of hand motions using ultrasound imaging of forearm muscles," *IEEE Transactions on Biomedical Engineering*, vol. 63, no. 8, pp. 1687–1698, 2015.

[47] Q. Zhang, K. Lambeth, Z. Sun, A. Dodson, X. Bao, and N. Sharma, "Evaluation of a fused sonomyography and electromyography-based

control on a cable-driven ankle exoskeleton," *IEEE Transactions on Robotics*, 2023.
[48] Z. Sheng, N. Sharma, and K. Kim, "Ultra-high-frame-rate ultrasound monitoring of muscle contractility changes due to neuromuscular electrical stimulation," *Annals of biomedical engineering*, vol. 49, pp. 262–275, 2021.
[49] ——, "Quantitative assessment of changes in muscle contractility due to fatigue during nmes: An ultrasound imaging approach," *IEEE Transactions on Biomedical Engineering*, vol. 67, no. 3, pp. 832–841, 2019.
[50] Z. Sheng, A. Iyer, Z. Sun, K. Kim, and N. Sharma, "A hybrid knee exoskeleton using real-time ultrasound-based muscle fatigue assessment," *IEEE/ASME Transactions on Mechatronics*, vol. 27, no. 4, pp. 1854–1862, 2022.
[51] A. Iyer, Z. Sun, K. Lambeth, M. Singh, C. Cleveland, and N. Sharma, "Real-time ultrasound imaging of a human muscle to optimize shared control in a hybrid exoskeleton," *IEEE Transactions on Robotics*, 2024.
[52] J. Ding, A. S. Wexler, and S. A. Binder-Macleod, "A predictive fatigue model. i. predicting the effect of stimulation frequency and pattern on fatigue," *IEEE Transactions on Neural Systems and Rehabilitation Engineering*, vol. 10, no. 1, pp. 48–58, 2002.
[53] R. Perumal, A. S. Wexler, and S. A. Binder-Macleod, "Mathematical model that predicts lower leg motion in response to electrical stimulation," *Journal of biomechanics*, vol. 39, no. 15, pp. 2826–2836, 2006.
[54] K. Graichen and B. Käpernick, *A real-time gradient method for nonlinear model predictive control*. INTECH Open Access Publisher London, 2012.
[55] A. Savitzky and M. J. Golay, "Smoothing and differentiation of data by simplified least squares procedures." *Analytical chemistry*, vol. 36, no. 8, pp. 1627–1639, 1964.
[56] V. Molazadeh, Q. Zhang, X. Bao, B. E. Dicianno, and N. Sharma, "Shared control of a powered exoskeleton and functional electrical stimulation using iterative learning," *Frontiers in Robotics and AI*, vol. 8, p. 711388, 2021.
[57] B. Xian, D. M. Dawson, M. S. de Queiroz, and J. Chen, "A continuous asymptotic tracking control strategy for uncertain nonlinear systems," *IEEE Transactions on Automatic Control*, vol. 49, no. 7, pp. 1206–1211, 2004.
[58] Z. Sun, X. Bao, Q. Zhang, K. Lambeth, and N. Sharma, "A tube-based model predictive control method for joint angle tracking with functional electrical stimulation and an electric motor assist," in *2021 American Control Conference (ACC)*. IEEE, 2021, pp. 1390–1395.
[59] B. W. Heller, A. J. Clarke, T. R. Good, T. J. Healey, S. Nair, E. J. Pratt, M. L. Reeves, J. M. van der Meulen, and A. T. Barker, "Automated setup of functional electrical stimulation for drop foot using a novel 64 channel prototype stimulator and electrode array: results from a gait-lab based study," *Medical engineering & physics*, vol. 35, no. 1, pp. 74–81, 2013.
[60] M. Singh, K. Lambeth, A. Iyer, and N. Sharma, "Dynamic active subspaces for model predictive allocation in over-actuated systems," *IEEE Control Systems Letters*, vol. 8, pp. 145–150, 2023.
[61] M. Singh, N. Hakam, T. M. Kesar, and N. Sharma, "Koopman-based model predictive control of functional electrical stimulation for ankle dorsiflexion and plantarflexion assistance," *IEEE Transactions on Neural Systems and Rehabilitation Engineering*, vol. 33, pp. 1252–1262, 2025.
[62] T.-G. La and L. H. Le, "Flexible and wearable ultrasound device for medical applications: A review on materials, structural designs, and current challenges," *Advanced Materials Technologies*, vol. 7, no. 3, p. 2100798, 2022.
[63] X. Xue, H. Wu, Q. Cai, M. Chen, S. Moon, Z. Huang, T. Kim, C. Peng, W. Feng, N. Sharma *et al.*, "Flexible ultrasonic transducers for wearable biomedical applications: A review on advanced materials, structural designs, and future prospects," *IEEE Transactions on Ultrasonics, Ferroelectrics, and Frequency Control*, vol. 71, no. 7, pp. 786–810, 2023.
[64] M. Singh and N. Sharma, "Data-driven model predictive control for drop foot correction," in *2023 American Control Conference (ACC)*. IEEE, 2023, pp. 2615–2620.
[65] C. M. Gregory and C. S. Bickel, "Recruitment patterns in human skeletal muscle during electrical stimulation," *Physical therapy*, vol. 85, no. 4, pp. 358–364, 2005.